

Topological Charge Switch in Active Multi-Core Fibers

Petra P. Beliĉev, Goran Gligorić, Aleksandra Maluckov, Ljupĉo HadŹievski,
and Sergei Turitsyn*

Topological properties can make light field remarkably robust to various external perturbations. The ability to control and change on demand topological characteristics of light paves the way to new interesting physical phenomena and applications. Here, numerical modelling design of the device based on active multi-core fiber that can change topological charge of the state of light has been proposed. The concept is based on the nonlinear dynamics of optical vortices in active multi-core optical fiber with linearly coupled cores, saturated gain, and constant linear losses. Results demonstrate that the proposed system can provide change of the topological charge of vortices.

1. Introduction

Data transfer and manipulation via pure all-optical networks is still a great challenge. Optical route between sources and detectors often cannot bypass opto-electronic conversion of signal in switching nodes therefore breaking the optical domain of data traffic. One of the possible solutions for surpassing this problem is usage of phase vortex modes as carriers of optical switch functions. (see [1])

Optical vortex is a special class of coherent localized waves characterized by energy and momentum flow of optical field around singularities (see, e.g., [2–11] and references therein).

Phase vortex beams carry orbital angular momentum (OAM) and are characterized by topological charge S . In discrete systems this quantity takes discrete values and can be related to a winding number of a spatial amplitude/phase structure having zero value at the pivot point of the vortex. Quantized topological charges provide extra robustness of vortex beams in sense of their stability despite presence of irregularities in the system.^[3] Their features

found many interesting applications in the field of optical manipulation,^[4] optical trapping,^[5] optical tweezers,^[6] microscopy,^[8] information transmission, and optical interconnects^[9,10] or optical passive/active vortex generators.^[11]

The optical vortices are closely linked to the field of topological photonics that has attracted a great deal of interest recently.^[12–14] In mathematics, topology explains and quantifies how a geometric object can dramatically transform its form without losing certain properties. Topologically protected phases emerge as a platform for dielectric

topological photonic crystals, later, they have been generalized to non-Hermitian systems with gain and/or loss. Active vortex photonic components, such as, for example, optical amplifiers, that may serve, for example, in high-power lasers, are of special interest due to their topological stability. In the presence of nonlinearity, total output power can be increased by several times while preserving vortex properties.^[15] Therefore, possibility to transfer data with optical field using on the top of the traditional coding over power, phase, frequency, and polarization a topological charge, triggers growing interest in studying various systems that support such topological carriers.

OAM switch has been reported in free-space using spatial light modulators (SLM),^[16] nonlinear metasurfaces^[17] and waveguide couplers,^[18] and the so called vortex fibers.^[19] Fast switch response has been achieved in systems based on whispering gallery modes for vortex generation, whereas choice of topological charge has been thermally controlled.^[20,21] Although versatile with arbitrary numbers of possible OAM switches, complexity of reconfigurable free-space data channels increases with the number of SLMs necessary for conversion.^[16] Additionally, multiple scatterings inevitable in free-space optics may violate angular phase patterns of vortex modes. Nonlinear based approaches^[17,18] and vortex fiber system^[19] offer possibility for OAM switch, but solely between corresponding counterpart phase vortices carrying topological charges $\pm S$.

One of the possible platforms for practical implementation of topological objects is technology of optical multi-core fibers (MCFs). It is actively developing as one of the possible approaches to implement spatial-division multiplexing (SDM) in future ultra-high-capacity optical communications. (see [22,23]) The MCFs support discrete optical vortices that carry OAM that might find a number of interesting applications beyond telecom, for instance in high power laser, power delivery, imaging, high-power amplifiers^[24,25] and laser processing of materials. (see, e.g., [26]) Theoretical analysis of stable discrete vortices carrying high

P. P. Beliĉev, G. Gligorić, A. Maluckov, Lj. HadŹievski
Department of Atomic Physics, "VINĀA" Institute of Nuclear Sciences
National Institute of the Republic of Serbia
University of Belgrade
P. O. B. 522, Belgrade 11001, Serbia

S. Turitsyn
Aston Institute of Photonic Technologies
Aston University
Birmingham B4 7ET, UK
E-mail: s.k.turitsyn@aston.ac.uk

S. Turitsyn
Aston-NSU Centre for Photonics
Novosibirsk State University
Novosibirsk 630090, Russia

 The ORCID identification number(s) for the author(s) of this article can be found under <https://doi.org/10.1002/andp.202100108>

DOI: 10.1002/andp.202100108

power in nonlinear MCFs has been presented in [15]. It has been shown that presence of a central core has no impact on vortex stability at high powers, while causes destabilization at intermediate power levels.

It should be stressed that nonlinearity imposes limits on coherent propagation. In optical communications, typically, fiber nonlinearity is considered as a factor leading to degradation of the quality of signal transmission and limiting performance of optical communication systems.^[27] However, nonlinear effects can be used to design and develop ultra-fast passive and active optical components and devices in which signal is controlled by light.^[28–30] In [31] theoretical analysis of coherent energy transfer through low-dimension nonlinear MCF was carried out. Using the intrinsic system symmetry to describing it through the effective two-core model it has been shown that power split between the cores comes from the nonlinear phase shift and is responsible for coherent propagation in MCF. Depending on the number of (in general nonequal) cores, input power, linear phase mismatch and ratio between nonlinearity coefficients, power split ratio and steady-state solutions can be determined. The additional influence of azimuthal perturbations and power sharing between periphery cores was studied in [32]. More detailed analysis including total number of cores within the model was presented in [33] where conditions for self-focusing of the beam in various cores have been found. In practical case, performances of afore mentioned high-power devices depend on various parameters of the system such as gain, loss, dispersion and nonlinearity which has been discussed in [25,34,35] and their choice is of crucial importance for guidance of coherent structures. Nonlinear solitary lightwave–optical soliton^[29] is an important example how nonlinearity can provide coherence of light for various practical applications from communications and laser to optical combs.

At high signal power MCF presents an example of nonlinear discrete physical system, interesting both for fundamental science^[15,31–34,36,37] and for various potential practical applications in nonlinear photonic devices.^[24,25,38–43] The case of loss-gain in MCFs in a discrete PT-symmetric configuration has also attracted attention recently.^[44–46]

We consider circular nonlinear active MCF as an example of compact photonic system providing multiple functions necessary for all-optical data transfer. The light propagation is analyzed via general model that includes effects of the saturable gain and non-saturable loss^[35] in the MCF cores. Through numerical analysis, we present phenomenon of power controlled topological charge switch among different discrete vortices relying on their stability patterns in passive nonlinear MCF. Merged impacts of core characteristics (gain, loss, and nonlinearity) distributed along the periphery give rise to generation of stable high-power vortex modes. These features could be exploited for practical realization of optical OAM switchers and vortex amplifiers. Refs. [16–21] already published their observations regarding this matter, but none examined fibers as a ground system to achieve topological charge switch between non-counterpart OAM states. Our analysis shows that MCF system supports greater range of “switchability” between the states when compared to other proposed photonic schemes. We stress discreteness as significant feature of MCFs ensuring stability of high power vortex modes, thus providing long-distance transfer joined with additional degree of freedom of information coding via topological charge switching. Addi-

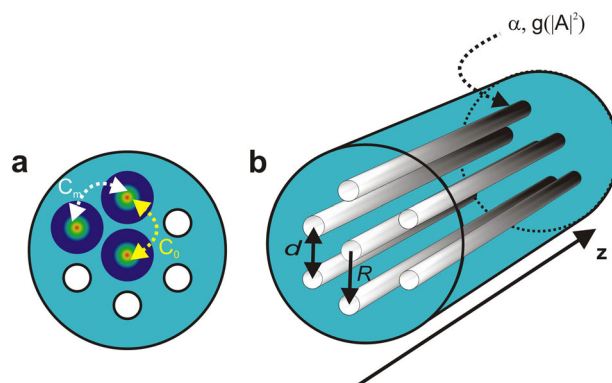


Figure 1. Schematic representation of nonlinear active MCF system with six periphery cores. a) Cross-section of hexagonal MCF depicting field coupling between individual cores and b) 3D perspective. C_0 and C_m stand for different strength of coupling between central-periphery and periphery-periphery cores, respectively. Coupling constants values obey $C_0 = C_1$ as a consequence of equality of geometrical parameters R and d . First is a central-periphery core distance while the second stands for the distance between two neighboring sites at the periphery. Loss α and gain g are material characteristic of the cores. Loss is constant along the propagation direction z . Gain is a function of the MCF mode's power.

tional advantages of presented results will be reflected through other operating regimes of MCF (gain distribution included in central core, too), serving as a platform for high-power fiber lasers or for coherent beam combining.

2. Model

A general case of circular MCF consisted of nonlinear active central and M periphery cores symmetrically distributed around the central one and all parallel to the z direction, is schematically shown in **Figure 1**.

In the framework of discrete optics models, coherent propagation of light through such system is governed by a set of differentially difference Ginzburg–Landau equations or nonlinear Schrödinger equations with complex coefficients:^[35]

$$i \frac{da_0}{dz} + \beta_0 a_0 + C_0 \sum_{m=1}^M a_m + 2\gamma_0 |a_0|^2 a_0 - i \left(\frac{G(a_0)}{2} - \frac{\alpha_0}{2} \right) a_0 = 0$$

$$i \frac{da_m}{dz} + \beta_m a_m + C_0 a_0 + C_m (a_{m+1} + a_{m-1}) + 2\gamma_m |a_m|^2 a_m - i \left(\frac{G(a_m)}{2} - \frac{\alpha_1}{2} \right) a_m = 0 \quad (1)$$

Here, a_0 and a_m stand for complex amplitude of the light field in the central and periphery cores, respectively, with corresponding linear propagation constants denoted as β_0 and β_m . Following the tight-binding approximation approach,^[47] weak evanescent field couplings among cores are described via coupling constants C_0 and C_m , as shown in **Figure 1a**. Higher-order couplings are presumed to be insignificant, so only the first-neighbor interactions are taken into account within the model. Due to ring distribution of periphery cores, we impose periodic boundary conditions meaning that the first $m = 1$ and last $m = M$ cores

are the nearest neighbors. Instantaneous nonlinear response of each core is of Kerr type whereas γ represents nonlinear parameter, while the power dependent (saturated) gain and effective distributed loss are given by G and α , respectively. Parameter distinction between central and periphery cores is made through subscripts 0 for central and m for periphery cores. The saturated gain is modelled in the following manner:

$$G(a_i) = \frac{g_i}{1 + |a_i|^2/E}, i \in [0, M] \quad (2)$$

with g_i being small signal gain and E representing saturation electrical field of the signal passing through the amplifying medium that saturates gain down to half value of g_i . Introducing substitution as $B_i = \beta_i + i\alpha_i/2$ which leads to complex notation of propagation constant, previous set of equations reduces to the following 1D version:

$$\begin{aligned} i \frac{d\Psi_0}{dz} + B_0\Psi_0 + C_0 \sum_{m=1}^M \Psi_m + 2\Gamma_0|\Psi_0|^2\Psi_0 - i\frac{g_0}{2} \frac{\Psi_0}{1 + |\Psi_0|^2} &= 0 \\ i \frac{d\Psi_m}{dz} + B_m\Psi_m + C_0\Psi_0 + C_m(\Psi_{m+1} + \Psi_{m-1}) + 2\Gamma_m|\Psi_m|^2\Psi_m \\ - i\frac{g_m}{2} \frac{\Psi_m}{1 + |\Psi_m|^2} &= 0 \end{aligned} \quad (3)$$

after taking the normalization $a_i = \sqrt{E}\Psi_i$ ($i \in [0, M]$). Adequately, the nonlinear term has been transformed into $\Gamma_i = \gamma_i E$.

Following severe analysis on the dynamically stable vortex solutions existing in the nonlinear MCF passive system,^[15] we get mathematical form of discrete vortices carrying topological charge S :

$$\Psi_0 = 0, \Psi_m = \Psi \exp(i \cdot 2\pi m S/M) \exp(-i\mu z), m \in [1, M] \quad (4)$$

where μ stands for the propagation constant of vortex solution, while phase difference between the vortex nodes equals $\Delta\phi = 2\pi S/M$. In general, light propagation in the passive MCF is characterized by the conservation of total power P and Hamiltonian H .^[48] The peculiarity of the vortices is the conservation of the momentum J , too:

$$P = \sum_{m=1}^M |\Psi_m|^2 \quad (5)$$

$$\begin{aligned} H = - \sum_{m=1}^M \left[-\beta_m |\Psi_m|^2 - C_1(\Psi_{m+1}\Psi_m^* + \Psi_{m+1}^*\Psi_m) \right. \\ \left. - C_0(\Psi_0\Psi_m^* + \Psi_0^*\Psi_m) - \Gamma_m |\Psi_m|^4 \right] - \beta_0 |\Psi_0|^2 - \Gamma_0 |\Psi_0|^4 \end{aligned} \quad (6)$$

$$J = i \sum_{m=1}^M (\Psi_m\Psi_{m+1}^* - \Psi_m^*\Psi_{m+1}) \quad (7)$$

Introduction of gain and loss terms within the model transforms MCF system into non-Hermitian, whereas P and H are

no longer conserved. Evolution of the momentum J follows the equation:

$$\frac{dJ}{dz} = \frac{2g\Psi^2}{1 + \Psi^2} \times M \sin\left(\frac{2\pi S}{M}\right) \quad (8)$$

implying conservation of momentum solely for vortices characterized by integer values of $2\frac{S}{M}$. Here, Ψ is the vortex amplitude.

In a case of vortex solution starting from Equation (3) and presuming equal loss (α) and gain (g) within all cores, it is possible to find evolution of total power with distance z as a function of loss and gain:

$$\frac{dP}{dz} = \left(-\alpha + \frac{g}{1 + P/M}\right)P \quad (9)$$

This equation has the solution presented in the form of the transcendent equation expressing power energy as a function of the propagation distance z along the MCF: (see, e.g., [35])

$$\frac{P(z)}{M} \times \left[1 - s \left(1 + \frac{P(z)}{M}\right)\right]^{-\frac{1}{s}} = \exp[(g - \alpha)(z - z_0)], \quad s = \frac{\alpha}{g} \quad (10)$$

Here z_0 is a conserved quantity (integral of motion) of Equation (9) that is determined by the initial value of the power at $z = 0$. It is seen that the asymptotic stationary value of the total power of vortex that will be achieved after transient time is:

$$P_{sat} = \left(\frac{g}{\alpha} - 1\right)M \quad (11)$$

Therefore, the new vortex steady state is characterized by amplitude $\Psi = \sqrt{g/\alpha - 1}$ which is determined by the gain/loss ratio. Pairs of gain/loss parameter values can be associated to the exceptional points which, in general, present the critical values in the non-Hermitian systems when Hamiltonian of the system is a real operator. The newly formed steady states' properties are investigated in the following. Regarding the circular MCF geometry (the central core and ring of periphery cores), we are specially interested in possibility to design the final steady state with non-zero vorticity by managing the input vortex modulation and system parameters.

Vortex modes families of particular topological charge found to exist in passive MCF system were used as initial trial solutions to Equation (3). Adequate numerical investigations of vortex solution dynamics have been conducted using the sixth-order Runge–Kutta numerical procedure^[49] by adding two types of small amplitude perturbations to the initial input: random and staggered (out-of-phase) amplitude perturbation. Following^[35] the ratio loss/gain has been observed in the range [0.01–1]. Three types of active circular MCFs have been analyzed: 1) MCF with gain distributed solely in periphery cores; 2) MCF with only central core being active and 3) MCF with all cores being active. When included, we set gain parameters g_0, g_m to be equal to 1 for the sake of simplicity.

3. Results and Discussion

In general, coupling coefficients in discrete optical systems are complex due to material losses that cannot be avoided especially

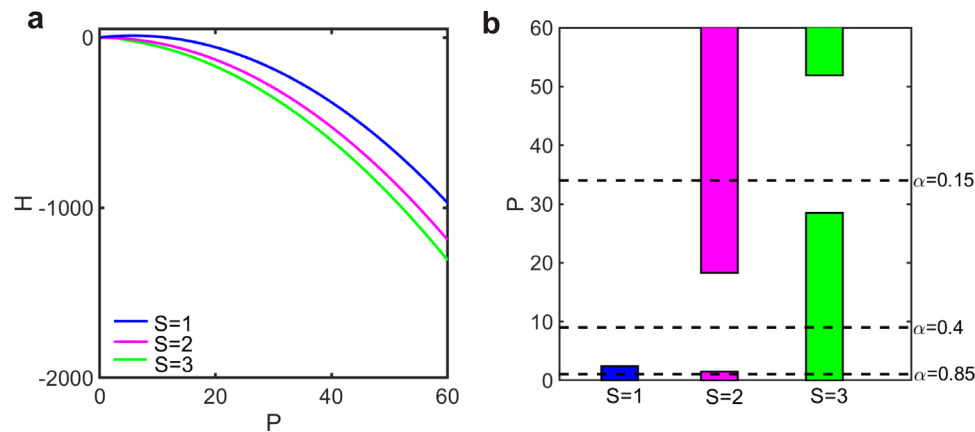


Figure 2. Optical vortex characteristics in nonlinear passive MCF system with $M = 6$ periphery cores: a) H-P diagram for vortex families characterized with topological charge $S = 1$, $S = 2$ and $S = 3$. b) Parallel overview of stability regions for corresponding vortex solutions. Colored bars depict areas where solution is stable. Horizontal black dashed lines represent output saturation power levels of vortices when gain and loss are included in periphery cores of the system.

in long transmission links. Detailed analysis on this issue have been done in [36,47] for silica based MCF showing that the losses are dominantly governed by the material absorption of the cores. Example presented here is MCF with $M = 6$ periphery cores. All cores possess equal linear parameters which are set to be $C_0 = C_m = \beta_0 = \beta_m = 1$. This assumption is valid having in mind hexagonal geometry where distance between any pair of neighboring identical cores is equal, as schematically shown in Figure 1. Presuming the same nonlinear response in each of the cores we take nonlinear parameters $\Gamma_0 = \Gamma_m = 1$ without loss of generality. All cores are considered to have equal losses, as well. We performed detailed analysis for $M = 4, 5$ and 6 cores and observations that follow are qualitatively the same for general case of MCFs with small number of periphery cores.

Hamiltonian-Power diagram of corresponding vortex families existing in passive MCF with $M = 6$ nodes is plotted in Figure 2a. It can be seen that solutions carrying $S = 3$ topological charge have lowest energy in the system. Solution families characterized with $S = 1$ and $S = 5$ are complementary cases. They reduce to the vortex with the same phase difference between the nodes, but rotating in opposite direction. These phase distributions in the vortex cross-section would correspond to counterpart phase vortices denoted as OAM_{+1} and OAM_{-1} found to be suitable for representation, that is, coding of binary data information.^[2] Same stands for solutions with $S = 2$ and $S = 4$. The phase counterpart modes are not directly related to the main stream of our study, so they are not considered in the following.

For illustration, comparative representation of the stability “windows” for steady state vortices carrying topological charge $S = 1$, $S = 2$ and $S = 3$ is given in Figure 2b for passive MCF. It is clear that all three families are characterized by one power instability window, whereas instability regions for $S = 2$ and $S = 3$ carriers do not overlap. Solutions characterized with $S = 1$ are unstable in almost whole region of existence ($P_{S1} > 2.4$, $\alpha_{S1} < 0.71$). Instability power windows found for other two families of vortices are $P_{S2} = (1.5 \text{ to } 18.3)$ ($\alpha_{S2} = (0.25 \text{ to } 0.8)$) and $P_{S3} = (28.2 \text{ to } 51.9)$ ($\alpha_{S3} = (0.1 \text{ to } 0.18)$).

Including loss and gain terms in the model equation we transform the existing system into an active one, that is, the one which

can produce power gain. The central core, that is, a pivot point of the vortex, which is empty in the passive system, plays a decisive role in the active case. By managing the pumping and loss mechanisms the central core can “silently” lead the active vortex dynamics or take a leading role in the coherent energy transfer. The dynamical steady state of the system will be therefore the vortex mode with enhanced power, or the zero-vorticity mode with huge energy, respectively. As will be shown in the following, the presence of gain in the periphery or central core significantly differentiates the system’s operating mode, and thus traces the MCF to different applications.

3.1. Pumping of Periphery Cores - Optical Vortex Switcher

As an initial step, we first observe case with gain distributed solely within the periphery cores ($g_0 = 0$ and $g_m = g_1 = 1$) and vary value of losses identically in all cores including the central one. As shown in Equation (11), saturation power of the steady state vortex mode will depend on the ratio g_1/α .

Based on the topological charge of the initial vortex solution and stability region in which saturation power of the evolved state “falls” in, we distinguish three possible scenarios: 1) preservation of topological charge; 2) topological charge switch, that is, transition to $S = 3$ vortex solution; 3) energy transfer to all cores of the system.

In active MCF, light behavior can be maintained by tuning the ratio between the gain and loss parameters. First scenario indicates preservation of topological charge with an increase of total output power of vortex mode. Numerical results show that this regime is governed by the position of saturated power P_{sat} for the observed topological charge vortex with respect to its power instability window. As long as P_{sat} remains in the stability window for the given vortex family, vortex mode power will be amplified and the topological charge will be preserved (bottom color bars in Figure 2b). Evolution of cores power and corresponding phase difference among periphery cores is plotted in Figure 3 for initially launched vortices with $S = 1$, $S = 2$ and $S = 3$ topological charge. It can be seen in Figure 2b that for $\alpha = 0.85$ all types of

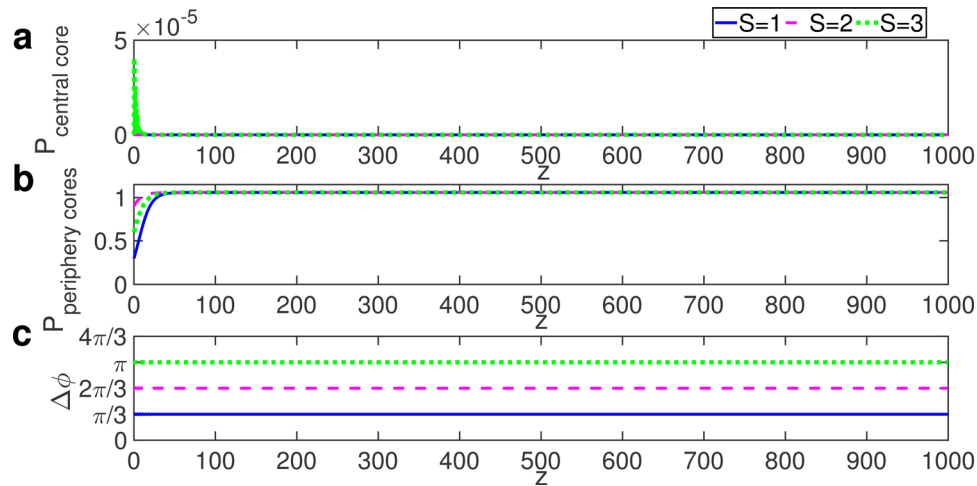


Figure 3. Evolution of power within central (a) and periphery cores (b). c) Phase difference between neighbouring periphery cores. Loss α is set to 0.85. Only periphery cores are active. Initially injected vortices are characterized with $S = 1$ and $P = 0.3$, $S = 2$ and $P = 0.9$ and $S = 3$ and $P = 0.6$, respectively. In all cases topological charge has been preserved during propagation.

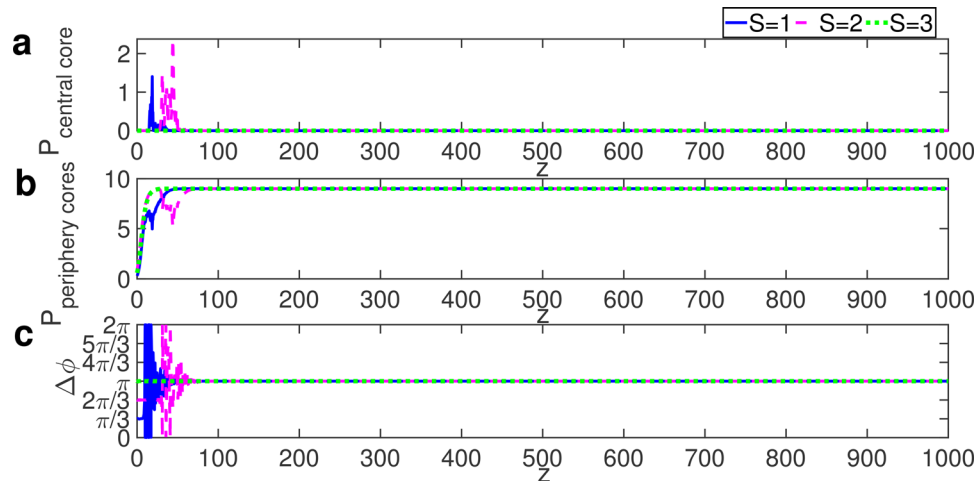


Figure 4. Evolution of power within central (a) and periphery cores (b). c) Phase difference between neighbouring periphery cores. Only periphery cores are active. Initially injected vortices are same as in Figure 3, while value of loss is set to $\alpha = 0.4$. Solutions $S = 1$ and $S = 2$ experience topological charge switch and transform to vortex mode $S = 3$ characterized with $\Delta\phi = \pi$.

vortices fulfill necessary stability conditions leading to the same output saturated power of $P_{sat} = 1.06$ in periphery (Figure 3b), but with phases rotating with different speeds (Figure 3c). During short transient period there is negligible coupling of energy into the central core as shown in Figure 3a, after which all energy is equally redistributed back to the periphery cores. For example, vortex with topological charge $S = 1$ will continue to propagate coherently with phase difference $\Delta\phi = \pi/3$, carrying around three times higher power than in the beginning. Higher power levels are possible to achieve for vortex families of topological charge $S = 2$ and $S = 3$ by choosing smaller losses which provide saturation powers within individual stability windows.

Second scenario refers to a quite interesting effect as an addition to the amplification of vortex power. For the range $\alpha \approx (0.25$ to $0.7)$ we reach saturation power levels corresponding to the instability power windows for $S = 1$ and $S = 2$ solutions. As shown in **Figure 4a**, transient period indicates more active participation

of the central core except for the solution $S = 3$ which is already stable in this area. In the case of other two vortex families, notable part of the energy from initially launched vortex modes couples to and then out from the central core, equally filling periphery cores (Figure 4b). The newly formed structure is vortex solution characterized with the phase difference of $\Delta\phi = \pi$ between neighboring nodes (see Figure 4c). Starting vortex experienced topological charge switch from $S = 1$ to $S = 3$ ($S = 2$ to $S = 3$) state, preserving coherence but with phase rotating faster around the pivot point. Due to the conditions determining instability within this power range, initial vortex moves into a more favorable energetic state, that is, vortex family solutions with topological charge $S = 3$. Therefore, response of the active system follows stability patterns of vortex solutions obtained for the case of nonlinear passive MCF with preference to the $S = 3$ solution corresponding the lowest H-P branch (the minimum Hamiltonian) as shown in Figure 2a. This phenomenon could be related to “repulsive”

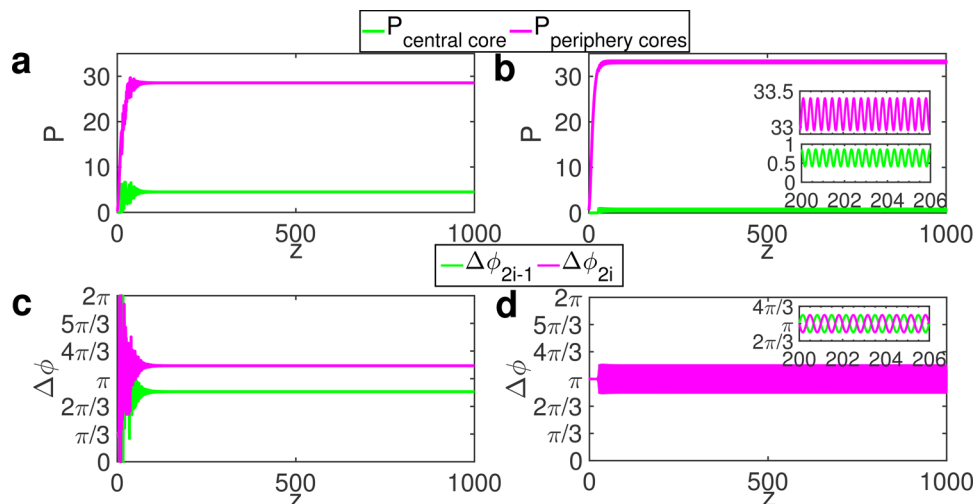


Figure 5. Evolution of total power within periphery (magenta solid line) and central core (green solid line) for initially injected vortex with a) $S = 1$ and $P = 0.3$, and b) $S = 3$ and $P = 0.6$. Corresponding evolution of phase difference among periphery cores are given in (c) and (d), respectively. Loss α is set to 0.15. Only periphery cores are active. Insets in plots (b) and (d) represent enlargement of related quantities.

tendency of the singular vortex point—the central core, which was initially empty and suddenly excited by energy leaking from the periphery. On the other hand, high values of loss in the central core cause coupling and redistribution of the energy back to the periphery cores. Here, the energy content is balanced among them tailoring the optimal vorticity of the propagating mode. Additionally, the initial angular momentum distribution protects vorticity allowing exchange of the topological charge from $S = 1$, that is, $S = 2$ to $S = 3$ for certain loss values.

For the range $\alpha \approx (0.18\text{--}0.25)$ the saturated powers of vortices $S = 2$ and $S = 3$ are in their stable regions. In this region, we observe transition of unstable vortex $S = 1$ to stable vortex $S = 3$, while vortices $S = 2$ and $S = 3$ keep their topological charge under the staggered type of perturbations. However, in the range nearby exchange of stability of vortices $S = 2$ ($\alpha = 0.25 \pm 0.05$), its dynamics is more sensitive to perturbation types and for random one the final state of launched $S = 2$ depends on its initial power and random perturbations realization. Nevertheless, for $\alpha > 0.3$ transition from $S = 2$ to $S = 3$ is unambiguous and does not depend on the type of perturbations (staggered or random) and its initial power. The only condition for transition is the presence of perturbations.

Finally, the last scenario covers the situation when starting solution saturates to the powers greater than 28.2. The presence of losses with values $\alpha < 0.18$ in the system will cause activation of central core, except in the case of vortex solutions $S = 2$ which will preserve phase difference of $\Delta\phi = 2\pi/3$ between neighboring nodes carrying up to 100 times larger power. On the other hand, solutions characterized with $S = 1$ topological charge experience nearly equal power split between central and periphery cores (see Figure 5a). Here, power in individual cores sets to constant value during the propagation with the phase difference between neighboring nodes taking two values as shown in Figure 5c. Green solid line stands for phase differences $\Delta\phi_{2i-1} = \phi_{2i} - \phi_{2i-1}$ and magenta one depicts $\Delta\phi_{2i} = \phi_{2i+1} - \phi_{2i}$, where $i = 1, 2, 3$. Due to circular geometry and periodic boundary conditions, $\phi_7 = \phi_1$. If we launch vortex with $S = 3$ topological charge,

again central core participates in the mode dynamics. Now the final mode acts as a breathing structure periodically exchanging energy between the central and periphery cores, whereas the energy is dominantly trapped within the periphery cores as depicted in Figure 5b. We again distinguish two values of $\Delta\phi$. Breathing behavior of the mode is present in the phase evolution, too. Phase difference between nodes periodically changes with the propagation keeping constant difference of π between the two phase levels indicating staggered profile of the field in the periphery.

3.2. Pumping of Central Core - High-Power MCF Laser

As the next step, we include gain term in the model which is related to pumping of energy within the central core. Terms describing losses are again kept both, within central and periphery cores, and varied identically.

With gain distribution present solely in the central core ($g_0 = 1$ and $g_1 = 0$), initially launched vortex destabilizes and regime of light transport through all cores occurs now for any of loss values. Similar behavior is noticed for all vortex family solutions. In order to classify different sub-regimes of energy transport, we introduce power imbalance parameter η representing ratio between power within the central core and total power in the periphery. Power values taken into account were chosen immediately after the transient regime. Performing numerical analysis and varying losses in the range $\alpha \in [0.1, 0.5]$ we again observed three possible scenarios.

Small values of losses ($\alpha < 0.25$) are followed by below unity power imbalance, that is, $\eta < 1$. This regime corresponds to highly irregular behavior of light coupling among all cores.

On the other hand, for $0.25 < \alpha < 0.33$ power imbalance is between $1 \leq \eta < 4/3$ and energy tends to redistribute among all cores whereas power distribution among periphery nodes is not equal as shown in Figure 6a. Additionally, after the transient period phase difference takes several values (Figure 6c).

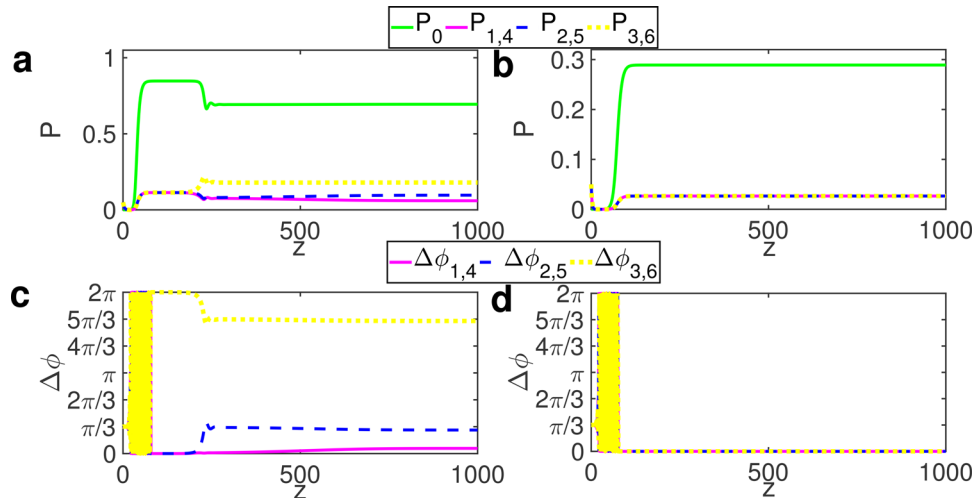


Figure 6. Evolution of power within central and periphery cores for $\alpha = 0.3$ (a) and $\alpha = 0.5$ (b), while only central core is active. Corresponding evolution of phase difference among periphery cores are given in (c) and (d), respectively. Initially launched vortex is characterized by $S = 1$ and $P = 0.3$.

With further increase of losses ($\alpha > 0.33$) the power imbalance parameter increases above $3/4$, and we observe that dominant part of energy has been localized at the central core, while the rest is equally redistributed among all periphery cores. As an example, case with $\alpha = 0.5$ is presented in Figure 6b. According to the $\Delta\phi$ plot, in-phase amplitude propagation within periphery cores is established (Figure 6d).

In this case, the MCF is “driven” to the dimerized, effective two-core system characterized by the zero-charge dynamical steady state with phase difference of π between the central and periphery cores, analogous to the passive two-core case of the MCF.^[31] Here, it has been proven that the coherent propagation in the effective two-core system is possible if the difference in the propagation constants is compensated by the nonlinear phase shifts. In such system the sensitive dependence on the imbalance between light intensity (power) propagating through the cores limits the parameter areas in which the stable coherent light propagation occurs. Contrary, the coherent propagation regime is shown reachable via the robust non-zero vorticity structured modes which are generically supported by the circular geometry of the system comprising central core.^[15] The vortex modes which are shown to be the eigenmodes of the nonlinear MCFs could be experimentally induced by proper phase arrangement of the input laser beam. The robustness of the vortices in active MCF is supported by proper gain/loss arrangement and geometry of the system, which is clearly shown in our numerical simulations. The critical point for the conversion of the mode topological charge from non-zero to zero value is reached by pumping the central core, that is, exciting the pivot (exceptional) point of the vortex structure. The central core converts from “silent” to leading power carrier in the system. The energetically favorable light formation is characterized by redistribution: the most of energy is localized in central core and the rest is equally shared by the periphery cores which behave as an entity. By managing the saturable nonlinear pumping and core losses the transition between different steady dynamical phases of light can be induced and controlled with huge implications in practice.

If we start with the full model of MCF system including all terms describing losses and gain within $M = 6$ plus central core configuration, then the relevant parameters are set to be $g_0 = g_1 = 1$.

Numerical results show that regarding the value of loss or topological charge of initially launched vortex, similar response always appears: $\Delta\phi$ among the periphery cores takes two constant values and newly created mode is characterized with almost equal power in each of the cores. Power carried by individual periphery core is slightly larger than power carried by central one. Value of α will have impact solely to the transient period after which system sets to a stable state; smaller the losses are longer it takes to reach saturation power level.

In general, with gain inclusion into the central core, fast energy transport and activation of an initially empty central core can be observed. Due to presence of gain, energy is amplified and the central core becomes equally effective energy transfer companion to the periphery ones. In the case of high loss regime and no gain present in the periphery cores ($\eta > 4/3$), MCF can be described via effective two core model. Especially this case offers possibility for transport of considerably huge power through the central core putting it as a promising candidate for highly efficient MCF laser.

4. Conclusion

We demonstrated a possibility to use MCF as a topological charge switch. We numerically examined propagation of phase vortex modes through nonlinear MCF system with constant (linear) loss and saturable gain within its cores. We studied three scenarios of gain distribution: solely in the peripheral cores, solely within central core and amplification in all cores of the MCF. We observed that initially empty central core always acts as a channel for energy coupling and redistribution among periphery cores of the system. The results for MCF with 4, 5, and 6 peripheral cores have shown that the case of amplifying peripheral cores is the most promising candidate for implementing topological charge switch.

When the gain is implemented only in the peripheral cores, we discovered that by suitable tailoring of loss and gain ratio in fiber cores it is possible to achieve the change of the vortex topological charge value, that is, transition between different vortex states. Depending on the stability region in which saturation power of the final state falls in, as well as on the topological charge of the initial vortex, evolved mode may transform to the vortex solution with energetically most preferable topological charge. For the case of $M = 6$ peripheral cores, it is the vortex state with topological charge $S = 3$. This topological charge “switch” protects vorticity of the propagating modes, thus providing robustness of coherent signal transfer to real-world imperfections which are inevitable during the fabrication processes of MCFs. For example, OAM-based reconfigurable optical switching functions have been reported in,^[16] where charge switch manipulation required spatial light modulators which make proposed schemes a bit complex and expensive. It should be stressed that the presented MCF system provides topological charge switch function between non-counterpart vortices by tuning the ratio between gain and loss in periphery. To the best of our knowledge, this phenomenon is for the first time observed in nonlinear media. On the top of this, switch function can be realized between high-power modes giving additional benefit in comparison to linear media.

The importance of central core, here, lays in its role of being the mode dynamics controller. As the singular phase point of vortex, which only passively takes part in tunneling energy towards the periphery cores, it can support coherent light amplification through the MCF. This points to a potential of presented system to be used as a high-power coherent source with possibility for selective topological charge manipulation of vortex beams. Additionally, MCF is an attractive platform for development of vortex beam generator system with a more simple design compared to the other controllable OAM mode generators.^[11]

When the gain is also present within the central core, light spreads among all cores with the tendency to trap the major fraction of the energy within the central core. By optimising the gain/loss ratio it is possible to achieve different operating regimes of MCF in terms of a total power split between the cores. Depending on the application, it is possible to provide coherent transport of substantial power mainly localized within the central core. The other regimes offer a possibility of a selective on demand distribution of energy between cores.

We have shown that initially launched power can be amplified for one or two orders of magnitude while keeping coherence and avoiding nonlinear instability. These results pave the way for another application of optical vortices in MCF, in high-power fiber lasers and coherent beam combiners.

From the power point of view, the “low ratio loss/gain” scenario offers possibility of stable and equal high-power transport through all cores in the system. However, it should be noted that the upper power limit is dictated by the characteristic damage limits of core materials.

Acknowledgements

This research was funded by the Ministry of Education, Science and Technological Development of Republic of Serbia. SKT acknowledges support from the Russian Science Foundation (Grant No. 17-72-30006).

Conflict of Interest

The authors declare no conflict of interest.

Data Availability Statement

Data sharing is not applicable to this article as no new data were created or analyzed in this study.

Keywords

light amplification, nonlinear active multi-core fiber, optical switch

Received: March 29, 2021

Revised: June 9, 2021

Published online:

- [1] A. Trichili, K.-H. Park, M. Zghal, B. S. Ooi, M.-S. Alouini, *IEEE Commun. Surv. Tutor.* **2019**, *21*, 3175.
- [2] J. Wang, *Photonics Res.* **2016**, *4*, B14.
- [3] M. Soskin, S. V. Boriskina, Y. Chong, M. R. Dennis, A. Desyatnikov, *J. Opt.* **2017**, *19*, 010401.
- [4] K. Dholakia, T. Čižmár, *Nat. Photonics* **2011**, *5*, 335.
- [5] L. Paterson, M. P. MacDonald, J. Arlt, W. Sibbett, P. E. Bryant, K. Dholakia, *Sci.* **2001**, *292*, 912.
- [6] M. J. Padgett, R. Bowman, *Nat. Photonics* **2011**, *5*, 343.
- [7] B. A. Malomed, *Physica D* **2019**, *399*, 108.
- [8] B. Spektor, A. Normatov, J. Shamir, *Appl. Opt.* **2008**, *4*, A78.
- [9] J. Wang, J.-Y. Yang, I. M. Fazal, N. Ahmed, Y. Yan, H. Huang, Y. X. Ren, Y. Yue, S. Dolinar, M. Tur, A. E. Willner, *Nat. Photonics* **2012**, *6*, 488.
- [10] A. E. Willner, H. Huang, Y. Yan, Y. Ren, N. Ahmed, G. Xie, C. Bao, L. Li, Y. Cao, Z. Zhao, J. Wang, M. P. J. Lavery, M. Tur, S. Ramachandran, A. F. Molisch, N. Ashrafi, S. Ashrafi, *Adv. Opt. Photonics* **2015**, *7*, 66.
- [11] Y. Shen, X. Wang, Z. Xie, C. Min, X. Fu, Q. Liu, M. Gong, X. Yuan, *Light Sci. Appl.* **2019**, *8*, 1.
- [12] L. Lu, J. Joannopoulos, M. Soljacic, *Nat. Photonics* **2014**, *8*, 821.
- [13] T. Ozawa, H. M. Price, A. Amo, N. Goldman, M. Hafezi, L. Lu, M. C. Rechtsman, D. Schuster, J. Simon, O. Zilberberg, I. Carusotto, *Rev. Mod. Phys.* **2019**, *91*, 015006.
- [14] M. A. Bandres, S. Wittek, G. Harari, M. Parto, J. Ren, M. Segev, D. N. Christodoulides, M. Khajavikhan, *Sci.* **2018**, *359*, eaar4005.
- [15] Lj. Hadžievski, A. Maluckov, A. M. Rubenchik, S. Turitsyn, *Light Sci. Appl.* **2015**, *4*, e314.
- [16] Y. Yue, H. Huang, N. Ahmed, Y. Yan, Y. Ren, G. Xie, D. Rogawski, M. Tur, A. E. Willner, *Opt. Lett.* **2013**, *38*, 5118.
- [17] Y. Xu, J. Sun, J. Frantz, M. I. Shalaev, W. Walasik, A. Pandey, J. D. Myers, R. Y. Bekele, A. Tsukernik, J. S. Sanghera, N. M. Litchinitser, *Appl. Sci.* **2019**, *9*, 958.
- [18] F. Diebel, D. Leykam, M. Boguslawski, P. Rose, C. Denz, A. S. Desyatnikov, *Appl. Phys. Lett.* **2014**, *104*, 261111.
- [19] N. Bozinovic, S. Golowich, P. Kristensen, S. Ramachandran, *Opt. Lett.* **2012**, *37*, 2451.
- [20] M. J. Strain, X. Cai, J. Wang, J. Zhu, D. B. Phillips, L. Chen, M. Lopez-Garcia, J. L. O'Brien, M. G. Thompson, M. Sorel, S. Yu, *Nat. Commun.* **2014**, *5*, 4856.
- [21] M. Scaffardi, M. N. Malik, J. Zhu, G. Goeger, N. Zhang, C. Klitis, Y. Ye, P. Rydlichowski, V. Toccafondo, M. Lavery, N. Andriolli, S. Yu, M. Sorel, A. Bogoni, in *2018 20th Int. Conf. on Transparent Optical Networks (ICTON)*, IEEE, Piscataway, NJ **2018**.

- [22] D. J. Richardson, J. M. Fini, L. E. Nelson, *Nat. Photonics* **2013**, *7*, 354.
- [23] R. G. H. van Uden, R. Amezcua Correa, E. Antonio Lopez, F. M. Huijskens, C. Xia, G. Li, A. Schülzgen, H. de Waardt, A. M. J. Koonen, C. M. Okonkwo, *Nat. Photonics* **2014**, *8*, 865.
- [24] K. Hizanidis, S. Droulias, I. Tsopelas, N. K. Efremidis, D. N. Christodoulides, *Phys. Scr.* **2004**, *T107*, 13.
- [25] K. Hizanidis, S. Droulias, I. Tsopelas, N. K. Efremidis, D. N. Christodoulides, *Int. J. Bifurc. Chaos Appl. Sci. Eng.* **2006**, *16*, 1739.
- [26] S. K. Turitsyn, V. K. Mezentsev, M. Dubov, A. M. Rubenchik, M. P. Fedoruk, E. V. Podivilov, *Opt. Express* **2015**, *15*, 14750.
- [27] A. D. Ellis, M. E. McCarthy, M. A. Z. Al Khateeb, M. Sorokina, N. J. Doran, *Adv. Opt. Photonics* **2017**, *9*, 429.
- [28] R. W. Boyd, *Nonlinear Optics*, 3rd ed., Academic Press, Boston, MA **2008**.
- [29] L. F. Mollenauer, J. P. Gordon, *Solitons in Optical Fibers: Fundamentals and Applications*, Academic Press, San Diego, CA **2006**.
- [30] C. Li, *Nonlinear Optics: Principles and Applications*, Shanghai Jiao Tong University Press and Springer Nature Pte Ltd., Shanghai **2017**.
- [31] S. K. Turitsyn, A. M. Rubenchik, M. P. Fedoruk, E. Tkachenko, *Phys. Rev. A* **2012**, *86*, 031804(R).
- [32] A. M. Rubenchik, E. V. Tkachenko, M. P. Fedoruk, S. K. Turitsyn, *Opt. Lett.* **2013**, *38*, 4232.
- [33] I. S. Chekhovskoy, M. A. Sorokina, A. M. Rubenchik, M. P. Fedoruk, S. K. Turitsyn, *IEEE Photonics J.* **2018**, *10*, 7101408.
- [34] A. J. Martínez, M. I. Molina, S. K. Turitsyn, Yu. S. Kivshar, *Phys. Rev. A* **2015**, *91*, 023822.
- [35] S. K. Turitsyn, *Opt. Express* **2009**, *17*, 11898.
- [36] A. Radosavljevic, A. Daničić, J. Petrović, A. Maluckov, Lj. Hadžievski, *J. Opt. Soc. Am. B* **2015**, *32*, 2520.
- [37] A. A. Balakin, A. G. Litvak, A. A. Skobelev, *Phys. Rev. A* **2019**, *100*, 053834.
- [38] Ph. Rigaud, V. Kermene, G. Bouwmans, L. Bigot, A. Desfarges-Berthelemot, *Opt. Express* **2015**, *23*, 27448.
- [39] A. Klenke, M. Müller, H. Stark, F. Stutzki, C. Hupel, T. Schreiber, A. Tünnermann, J. Limpert, *Opt. Lett.* **2018**, *43*, 1519.
- [40] C. Agger, S. T. Sørensen, C. L. Thomsen, S. R. Keiding, O. Bang, *Opt. Lett.* **2011**, *36*, 2596.
- [41] I. S. Chekhovskoy, A. M. Rubenchik, O. V. Shtyrina, M. P. Fedoruk, S. K. Turitsyn, *Phys. Rev. A* **2016**, *94*, 043848.
- [42] Y. Kim, S. C. Warren, J. M. Stone, J. C. Knight, M. A. A. Neil, C. Pater-son, C. W. Dunsby, P. M. W. French, *IEEE J. Sel. Top. Quantum Electron.* **2016**, *22*, 171.
- [43] S. García, I. Gasulla, *Opt. Express* **2016**, *24*, 20641.
- [44] S. Longhi, *Opt. Lett.* **2016**, *41*, 1897.
- [45] C. Castro-Castro, Y. Shen, G. Srinivasan, A. B. Aceves, P. G. Kevrekidis, *J. Nonlinear Opt. Phys. Mater.* **2016**, *25*, 1650042.
- [46] X. Zhang, V. A. Vysloukh, Y. V. Kartashov, X. Chen, F. Ye, M. R. Belic, *Opt. Lett.* **2017**, *42*, 2972.
- [47] M. Golshani, S. Weimann, K. Jafari, M. Khazaei Nezhad, A. Langari, A. R. Bahrapour, S. M. Mahdavi, A. Szameit, *Phys. Rev. Lett.* **2014**, *113*, 123903.
- [48] D. E. Pelinovsky, *Nonlinearity* **2006**, *19*, 2695.
- [49] W. H. Press, S. A. Teukolsky, W. T. Vetterling, B. P. Flannery, *Numerical Recipes: The Art of Scientific Computing*, 3rd ed., Cambridge University Press, New York **2007**.